# Orientational order and micelle size in the nematic phase of the cesium pentadecafluorooctanoate–water system from the anisotropic self-diffusion of water

Haukur Jóhannesson, István Furó,* and Bertil Halle
*Condensed Matter Magnetic Resonance Group, Chemical Center, Lund University, P.O. Box 124, S-22100 Lund, Sweden*
(Received 31 October 1995)

The self-diffusion of water in the nematic micellar phase of the cesium pentadecafluorooctanoate-water system has been studied by means of the $^2$H pulsed gradient spin echo NMR technique. The principal components of the macroscopic diffusion tensor were determined to high accuracy as functions of temperature and concentration. The orientational order parameter and the size of the discoidal micelles were derived from the data with the aid of a theoretical description of the obstruction and hydration effects, the accuracy of which was tested by stochastic simulations. While supporting the discrete-micelle model of the microstructure in the nematic phase, our results are in qualitative disagreement with previous interpretations of scattering and conductivity data as well as with theoretical predictions based on a hard-particle model. Our results thus indicate that the strong increase of orientational order with decreasing temperature is due to soft micelle-micelle interactions, presumably the anisotropic electrical double-layer repulsion, rather than to a growth-alignment coupling. On increasing the concentration at fixed relative temperature, we find that the micelle size increases while the orientational order decreases. The latter trend is rationalized in terms of the quadrupole-quadrupole component of the electrical double-layer interaction, which tends to destroy the orientational order.

PACS number(s): 61.30.Eb, 61.30.Gd, 64.70.Md, 66.10.Cb

## I. INTRODUCTION

Since its discovery in 1967 [1], the nematic micellar phase has been found in many binary and ternary amphiphile-water systems. This phase differs from its more familiar, molecular (thermotropic) counterpart in that the size and shape of the nematogenic unit, the micellar aggregate of amphiphilic molecules, may vary with temperature and concentration. To characterize the microscopic state of a nematic micellar phase, one must therefore determine not only the orientational order parameter of the micelles but also their size and shape.

The most thoroughly studied nematic micellar phase is probably that in the cesium perfluorooctanoate-(CsPFO-)water system [2]. This binary system exhibits a diamagnetically positive, discotic nematic phase that is stable over wide ranges of temperature (285.3–351.2 K) and concentration (micelle volume fraction, $\phi$=0.114–0.426) [3,4]. A variety of experimental techniques, primarily x-ray and neutron scattering [5–9], electrical conductivity [5,10–15], NMR spectroscopy [3–5], and water self-diffusion [16–18], have been used to study this nematic phase as well as the adjoining lamellar phase. A major conclusion, supported by many of these studies, is that the microstructure of the nematic phase changes relatively little with temperature. Moreover, the onset of long-range orientational and translational order at the isotropic-to-nematic ($I$-$N$) and nematic-to-lamellar ($N$-$L$) phase transitions, respectively, appear not to be accompanied by significant structural change [2,5]. Although the microstructure cannot be uniquely determined by any of the techniques mentioned, an oblate-spheroidal micelle is usually invoked as the basic structural unit in all three phases. Some authors have challenged this view, suggesting that the lamellar phase consists of amphiphile-continuous bilayers pierced by aqueous channels [7–9,13,14]. The question then arises whether the transition from discrete discoidal micelles to perforated bilayers occurs abruptly at the $N$-$L$ transition, which appears to be continuous over much of its concentration range [3,4], or continuously within the nematic and/or lamellar phases. On the basis of scattering data, Holmes, Leaver, and Smith recently argued for profound changes in microstructure within the nematic phase [9].

To address these controversial issues, we report here the results of an extensive study, by means of the $^2$H pulsed gradient spin echo (PGSE) NMR technique, of water diffusion in the nematic phase of the CsPFO-$D_2O$ system. As with all other techniques applied to this problem, the water diffusion approach suffers to some extent from model dependence. Since different techniques probe different aspects of the microstructure, however, we believe that the present diffusion data add important new information.

As compared to previous water diffusion studies of the nematic and lamellar phases, the present one differs in two important respects. First, by meticulously paying attention to all known potential sources of systematic error, we were able to reduce the experimental error to below 0.5% in the individual components of the diffusion tensor [19]. With this experimental accuracy, it is possible to detect even small variations in microstructure. Second, for the adopted microstructural model of oblate-spheroidal micelles, the obstruction and hydration effects on the measured water diffusion coefficients are described by new theoretical relations, the high accuracy of which has been confirmed by means of stochastic simulations [20].

The present results provide strong evidence for an essentially invariant microstructure of discoidal micelles, whose

*Present address: Division of Physical Chemistry, Royal Institute of Technology, S-10044 Stockholm, Sweden.

 

TABLE I. Compositions and transition temperatures of CsPFO-$D_2O$ samples investigated by water diffusion measurements.

| $w$[a] | $\phi$[b] | $N_w$[c] | $T_{NI}$/K[d] |
|---|---|---|---|
| 0.358 | 0.197 | 48.9 | 301.05 |
| 0.400 | 0.227 | 40.9 | 306.90[e] |
| 0.424 | 0.244 | 37.0 | 310.00 |
| 0.473 | 0.283 | 30.4 | 318.35 |
| 0.502 | 0.307 | 27.0 | 323.60 |

[a]Weight fraction CsPFO.
[b]Volume fraction CsPFO, calculated as $\phi=[1+2.275(1-w)/w]^{-1}$.
[c]Mole ratio $D_2O$-CsPFO.
[d]While the relative temperatures, $T-T_{NI}$, used in this work are accurate to 50 mK, the absolute transition temperatures given here may be systematically offset by 0.5–1 K.
[e]For this sample, $T_{NL}=301.1\pm0.1$ K.

size varies little with temperature, even on traversing the phase boundaries. Our results also shed new light on the variation of micelle size and orientational order with concentration. As the micelle volume fraction is increased at a fixed reduced temperature, we find that the micelles grow while the orientational order is diminished. Both of these trends are opposite to what has been inferred from scattering and conductivity data [2,5,6,9]. Our water diffusion data also imply that the anisotropy of the electrical conductivity, previously used to determine the orientational order parameter [2,5,10,11], is significantly affected by local electric fields.

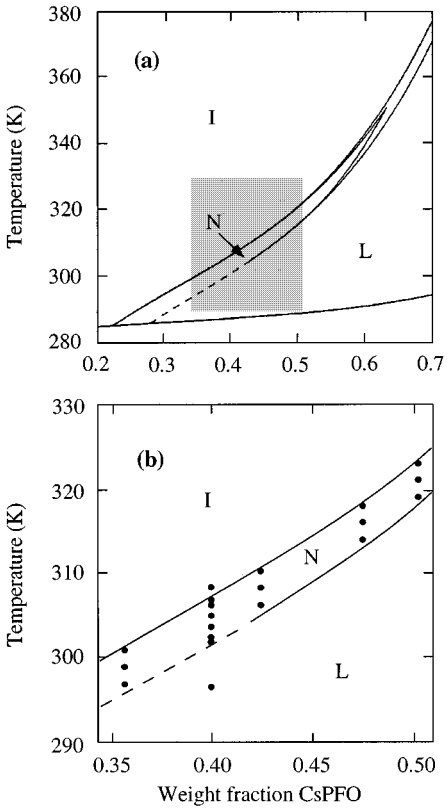


FIG. 1. (a) Partial phase diagram for the CsPFO-$D_2O$ system, taken from Ref. [4], showing the isotropic-to-nematic and nematic-to-lamellar transition curves and the solubility curve. Along the dashed curve, a two-phase region has so far not been detected [4]. (b) Enlargement of the shaded area in (a), showing the 20 investigated sample points.

## II. EXPERIMENT

### A. Materials and samples

Cesium pentadecafluorooctanoate (CsPFO) was prepared by neutralizing a 10 wt % aqueous solution of pentadecafluorooctanoic acid with a 30 wt % aqueous solution of CsOH at 40 °C. Recrystallization from *n*-butanol yielded white, glossy, flakelike crystals, indicative of a high degree of purity.

The samples were prepared by weighing CsPFO and $D_2O$ into glass vials, which were then flame sealed. After thorough mixing at ca. 50 °C, where all samples were isotropic, the mixture was transferred by syringe into 5-mm o.d. NMR tubes with the open end drawn out to form a long narrow neck (1 mm i.d.) above the sample containing part of ca. 16-mm height. To avoid thermal decomposition of CsPFO, the neck was flame sealed ca. 10 mm above the fluid level. Capillary forces ensured that the included air remained in the neck when the sample was horizontally placed in the NMR probe.

Table I lists the compositions, amphiphile volume fractions ($\phi$), and transition temperatures of the five investigated samples. The $N$-$I$ transition temperature $T_{NI}$ was determined from the appearance of a central line in the water $^2$H NMR spectrum, while the $N$-$L$ transition temperature $T_{NL}$ was obtained (at one composition) by cooling the sample into the lamellar phase outside the magnet and observing the transition from an isotropic powder spectrum to a doublet spectrum characteristic of a homeotropically aligned nematic phase [3]. Diffusion data were collected at 18 system points $(T,\phi)$ in the nematic phase, as well as at two points in the isotropic and lamellar phases. The locations of these system points are marked in the partial phase diagram of Fig. 1. The temperature range of the nematic phase is 5–6 K for the investigated samples.

The sample temperature in the NMR probe was regulated by a temperature controller (Stelar VTC87), with the flow of precooled air stabilized by a mass flow controller (MKS 1562A). The sample temperature was calibrated to a relative accuracy of 50 mK with the aid of the strongly temperature dependent water $^2$H quadrupole splitting (cf. Sec. IV D). The temperature gradient across the active sample volume was estimated to less than 60 mK. Since the relative temperature $T-T_{NI}$ is the essential variable in the present study, we made no attempt to calibrate the absolute temperature measurements to better than 1 K accuracy. Indeed, our nominal phase boundaries are 0.5–1 K below those reported by Boden and co-workers [3,4].

To avoid artifacts due to the formation of nonequilibrium defects [12,21], all measurements in the nematic phase were done on samples that had been cooled directly from the isotropic phase with the cylindrical sample axis perpendicular to the main magnetic field [21]. After each change of temperature, ca. 30 min thermal equilibration was allowed before the measurements.

### B. NMR diffusion measurements

The water self-diffusion measurements were performed on the $^2$H resonance of $D_2O$ using a Bruker MSL-100 NMR spectrometer equipped with a home-built diffusion probe and gradient power supply. The design and performance of this probe have been described in detail elsewhere [19]. To determine the principal components, $D_{\parallel}^{C}$ and $D_{\perp}^{C}$, of the macroscopic self-diffusion tensor, we used two probe inserts with fixed quadrupole coils that produce field gradients parallel and perpendicular to the direction of the main magnetic field and, hence, to the director (or optic axis) of the diamagnetically positive, uniaxial liquid-crystalline phases of the CsPFO-water system. The relative diffusion coefficients, $D_{\parallel}^{C}/D_0$ and $D_{\perp}^{C}/D_0$, which contain the desired microstructural information, were obtained by also measuring the bulk $D_2O$ diffusion coefficient, $D_0$, with each probe insert, thus obviating the need for an absolute calibration of the gradient coils.

Whereas most previous NMR studies of water diffusion have utilized the proton resonance, we chose to use the $^2$H nucleus for this study. Despite its lower NMR sensitivity, this nucleus is preferable since it allows much shorter recycling times (due to faster spin relaxation) and since potential artifacts (e.g., due to radiation damping) are avoided. Since $^2$H is a spin-1 nucleus, we employed the quadrupolar version of the conventional PGSE sequence, i.e., a $\pi/2$-$\tau$-$\pi/2$ quadrupolar echo sequence with two gradient pulses inserted [22–24]. The echo intensity $I(\delta)$ decays in the same way as in the conventional PGSE experiment, i.e. [22–24],

$$I(\delta)=I(0)\exp[-(\gamma\delta G)^2 D_{\alpha}^{C}(\Delta-\delta/3)], \qquad (2.1)$$

with $D_{\alpha}^{C}=D_{\parallel}^{C}$ or $D_{\perp}^{C}$ depending on the gradient coil orientation. Gradient pulses of strength $G\approx 0.40$ T m$^{-1}$, duration $\delta=1$–$10$ ms, and spacing $\Delta=60$ ms were applied. The echo decay was found to be unaffected by variations of $\Delta$, as expected for macroscopically unrestricted diffusion.

Fourier transformation of the free induction decay following the echo, which appears at a time $\tau$ after the second $\pi/2$ pulse, produced a doublet spectrum from which $I(\delta)$ was determined by integrating the central 80% of the two satellite peaks (of width 1–2 Hz). The quadrupole splitting $\nu_Q$ was also obtained from this spectrum as the frequency separation of the two peaks. The diffusion coefficient was finally determined from a nonlinear least-squares fit (Levenberg-Marquardt) to Eq. (2.1), as illustrated in Fig. 2.

The precision (random error) obtained from the fits was typically 0.2–0.3%. The accuracy (systematic error) was assessed by comparing measurements on the same sample with the PGSE method described above and with the constant-gradient CPTG-OE method [25]. The results coincided within their precision. We estimate the overall experimental uncertainty in $D_{\parallel}^{C}/D_0$ and $D_{\perp}^{C}/D_0$ to less than 0.5%. This rather exceptional accuracy, achieved by carefully minimizing all known sources of systematic error [19], proved essential for a quantitative determination of the microstructure in the nematic phase. For reference, a 1% error in the relative diffusion coefficients propagates into a 20% uncertainty in the micelle volume. The high accuracy of our data is evident from Fig. 3, showing the temperature dependence of the relative diffusion coefficients across the three phases.

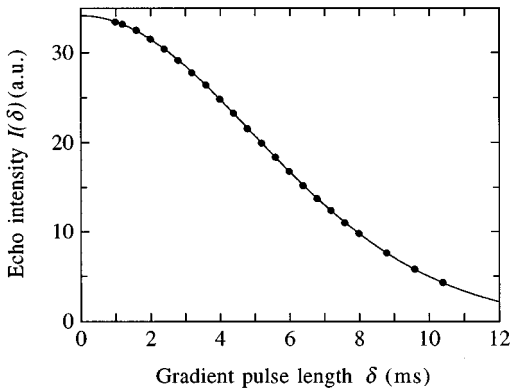


FIG. 2. Decay of the $^2$H satellite intensity in a PGSE experiment on a nematic sample ($\phi=0.227$, $T=T_{NI}-3.65$ K). The curve resulted from a fit to Eq. (2.1).

## III. WATER DIFFUSION IN A DISCOTIC NEMATIC PHASE

### A. Diffusion tensor

For a molecule in a uniaxial phase, such as a water molecule in a nematic $N_D^+$ phase, the experimentally accessible, macroscopic self-diffusion tensor **D** has two distinct principal components, $D_{\parallel}^{C}$ and $D_{\perp}^{C}$, referring to diffusion parallel and perpendicular to the director, respectively. These two observables contain information about the orientational order and the shape of the amphiphilic aggregates of the phase.

For simplicity, and in the absence of experimental evidence to the contrary, we assume that the aggregates are uniaxial or, at least, possess threefold symmetry. The orientational order of the nematic phase is then fully characterized by the distribution, $f(\theta)$, of the angle $\theta$ between the micellar symmetry axis and the director. Being components of a second-rank tensor, the diffusion coefficients can depend only on the lowest nonzero moment of this distribution, the second-rank orientational order parameter [26]

$$S=\langle P_2(\cos\theta)\rangle. \qquad (3.1)$$

By transforming the crystal-frame diffusion coefficients to

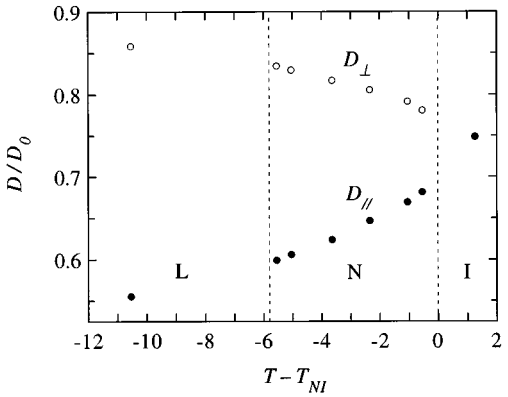


FIG. 3. Temperature variation of the relative water self-diffusion coefficients parallel (●) and perpendicular (○) to the director for the $\phi=0.227$ sample in the lamellar ($L$), nematic ($N$), and isotropic ($I$) phases. The error bars are the same size as the symbols.

a micelle-fixed frame, their dependence on $S$ can be made explicit. Since the trace of a symmetric tensor is invariant under an orthogonal transformation, we have

$$D_{\rm iso} \equiv \tfrac{1}{3}\,\mathrm{Tr}\,\mathbf{D} = \tfrac{1}{3}D_{\parallel}^{M} + \tfrac{2}{3}D_{\perp}^{M}. \tag{3.2}$$

Furthermore, since the traceless tensor $\mathbf{D} - D_{\rm iso}\mathbf{1}$ transforms as an irreducible second-rank tensor, it follows that

$$D_{\parallel}^{C} - D_{\rm iso} = S(D_{\parallel}^{M} - D_{\rm iso}). \tag{3.3}$$

In the subsequent analysis, we shall consider as experimental variables, not $D_{\parallel}^{C}$ and $D_{\perp}^{C}$, but rather the isotropic average $D_{\rm iso}$ and the (crystal-frame) diffusion anisotropy $\alpha_C$, defined as

$$\alpha_C \equiv \frac{D_{\parallel}^{C} - D_{\perp}^{C}}{D_{\rm iso}}. \tag{3.4}$$

These variables allow qualitative conclusions to be drawn about the microstructure of the phase without invoking a geometrical model. This is possible since the rotationally invariant $D_{\rm iso}$ is independent of the orientational order, while $\alpha_C$ is directly proportional to the order parameter. Indeed, according to Eqs. (3.2)–(3.4),

$$\alpha_C = S\alpha_M, \tag{3.5}$$

with

$$\alpha_M = \frac{3(D_{\parallel}^{M} - D_{\perp}^{M})}{D_{\parallel}^{M} + 2D_{\perp}^{M}}. \tag{3.6}$$

### B. Obstruction effect

The available information about micelle shape is contained in the micelle-frame diffusion coefficients $D_{\parallel}^{M}$ and $D_{\perp}^{M}$. If hydration effects are neglected (cf. Sec. III C), the local water diffusion coefficient is uniform throughout the free volume outside the micelles and equal to the bulk water diffusion coefficient $D_0$. The relative diffusion coefficients $D_{\parallel}^{M}/D_0$ and $D_{\perp}^{M}/D_0$ can then be interpreted as obstruction (or tortuosity) factors, describing the obstruction of the diffusion trajectory of a water molecule by the impenetrable micelles. For lamellar and discotic nematic phases, the following model-independent bounds apply in the absence of hydration effects:

$$\tfrac{2}{3} \leqslant D_{\rm iso}/D_0 \leqslant 1/(1+\phi/2), \tag{3.7}$$

$$-\tfrac{3}{2} \leqslant \alpha_M \leqslant 0. \tag{3.8}$$

The lower bounds correspond to a defect-free lamellar geometry, where $D_{\parallel}^{M} = 0$ and $D_{\perp}^{M} = D_0$, and the upper bounds to spherical micelles, where $D_{\parallel}^{M} = D_{\perp}^{M}$. (The upper bound on $D_{\rm iso}/D_0$ is strictly valid only for micelles on a periodic lattice [27].)

The obstruction factors depend on the volume fraction ($\phi$), shape, and spatial distribution of the micelles. To quantify the dependence on micelle shape, a geometric model must be specified. Although there is some controversy about the microstructure of the investigated nematic phase (cf. Sec. V), we shall adopt the conventional view [2] and model the micelles as monodisperse oblate spheroids.

While exact, closed-form expressions for the obstruction factors, valid over the full range of volume fractions, are not available for any nontrivial geometry, analytical approximations of the mean-field type have been obtained for spheroidal geometry [28,29]. In particular, the effective cell approximation (ECA) yields the simple results [29]

$$D_{\parallel}^{M}/D_0 = \frac{1}{1-\phi}\left(1 - \frac{\phi}{1 - h_m + \phi h_c}\right), \tag{3.9a}$$

$$D_{\perp}^{M}/D_0 = \frac{1}{1-\phi}\left(1 - \frac{2\phi}{1 + h_m + \phi(1 - h_c)}\right), \tag{3.9b}$$

where

$$h \equiv h(\xi) = (\xi^2 + 1)(1 - \xi\ \mathrm{arccot}\,\xi). \tag{3.10}$$

Here $\xi$ is the dimensionless "radial" oblate-spheroidal coordinate, taking the value $\xi_m$ at the micelle surface and the value $\xi_c$ at the external boundary of the confocal cell. The aspect ratio, $\rho = a/b$, with $a$ and $b$ the major and minor semiaxes of the oblate spheroid, respectively, determines $\xi_m$ according to

$$\xi_m = (\rho^2 - 1)^{-1/2}. \tag{3.11}$$

In the ECA, concentration effects are accounted for in a mean-field fashion by solving the steady-state diffusion equation in a spheroidal cell confocal with the micelle [29]. The cell volume is fixed by equating the micelle volume fraction in the cell with the macroscopic volume fraction, $\phi$, whereby $\xi_c$ is given by

$$\xi_c(\xi_c^2 + 1) = \frac{\rho^2}{\phi(\rho^2 - 1)^{3/2}}. \tag{3.12}$$

The micelle-frame diffusion anisotropy $\alpha_M$ varies strongly with the aspect ratio $\rho$ under the conditions of interest here (cf. below). The quantity $D_{\rm iso}/D_0$ varies relatively less, but if accurately determined can nevertheless be used to determine $\rho$ (cf. Sec. IV).

The accuracy of the mean-field approximation, Eqs. (3.9)–(3.12), has recently been assessed by means of stochastic simulations [20]. For oblate spheroids, the ECA was found to be quantitatively accurate up to $\phi \approx 0.5$ for $D_{\rm iso}/D_0$ and up to $\phi \approx 0.2$ for $\alpha_M$. The high accuracy is partly fortuitous, resulting from a cancellation of errors in $D_{\parallel}^{M}$ and $D_{\perp}^{M}$. For the most concentrated sample investigated here ($\phi = 0.307$), the ECA overestimates $-\alpha_M$ by a few percent, which, however, is negligible compared to the propagated experimental error in the order parameter $S$ determined from $\alpha_C$ (cf. Sec. IV). For the present data, the ECA is thus sufficiently accurate.

The simulation study also addressed the issue of model dependence by comparing the obstruction factors of oblate spheroids and hemitoroidal disks of the same aspect ratio [20]. At $\phi \approx 0.3$, no significant difference between the two geometries was found for $D_{\rm iso}/D_0$, while $-\alpha_M$ was 10–20% smaller (depending on the aspect ratio) for the disks.

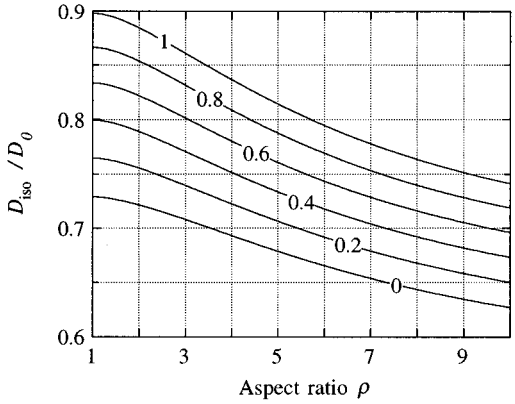


FIG. 4. Shape dependence of the isotropic diffusion coefficient, $D_{iso}/D_0$, for oblate spheroids at volume fraction $\phi=0.227$ according to the ECA with $n=6$ and $D_1/D_0$ as indicated.

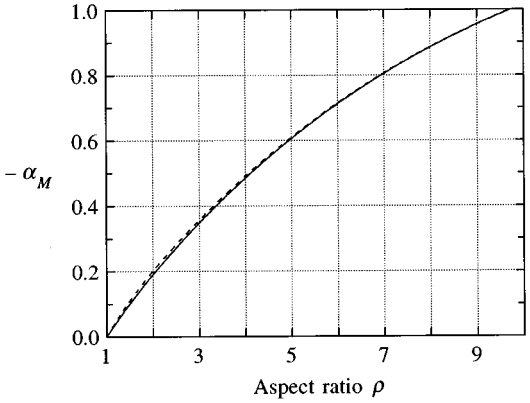


FIG. 5. Shape dependence of the micelle-frame diffusion anisotropy $\alpha_M$ for oblate spheroids at $\phi=0.227$ according to the ECA with $n=6$ and $D_1/D_0=1$ (solid curve) or $D_1/D_0=0$ (dashed curve).

### C. Hydration effect

In a real nematic micellar phase, interactions and steric effects at the micelle surface are expected to reduce the local diffusion coefficient for water molecules in contact with headgroups and associated counterions by a factor 2–3 or so. In the ECA treatment, this dynamic hydration effect can be modeled by assigning a reduced local diffusion coefficient, $D_1<D_0$, to water molecules residing in a confocal spheroidal shell at the micelle surface. Proceeding as in the case of spherical geometry [29], we have derived closed-form expressions for the reduced micelle-frame diffusion coefficients $D_{\parallel}^{M}/D_0$ and $D_{\perp}^{M}/D_0$ for hydrated oblate spheroids. These results are presented in Appendix A. Stochastic simulation results, reported in Appendix B, demonstrate that these analytical approximations are highly accurate under the conditions of the present study.

The reduced micelle-frame diffusion coefficients now depend, not only on $\phi$ and $\rho$, but also on two parameters that specify the magnitude and range of the dynamic hydration effect. These parameters are conveniently chosen as the local diffusivity ratio, $D_1/D_0$, and the "hydration number," $n$, giving the number of dynamically perturbed water molecules per CsPFO molecule. The calculated hydration effects on $D_{iso}/D_0$ and $\alpha_M$ are shown in Figs. 4 and 5. As a result of a nearly complete cancellation in Eq. (3.6), $\alpha_M$ is virtually unaffected by hydration. (For $\phi=0.25$, $\rho=4$, and $n=6$, $-\alpha_M$ decreases by merely 1.3% as $D_1/D_0$ varies from 0 to 1.) In contrast, $D_{iso}/D_0$ depends strongly on hydration. (At fixed $n$, $D_{iso}/D_0$ increases essentially linearly with $D_1/D_0$.)

Within the $\phi$ and $\rho$ ranges of interest here, the functional dependence of $D_{iso}/D_0$ on $\phi$ and $\rho$ is virtually the same for an infinite set of $(n,D_1/D_0)$ pairs. This behavior, previously noted for spherical obstructions [30], implies that $n$ and $D_1/D_0$ cannot be individually determined from diffusion data in this region of parameter space. Conversely, a single hydration parameter suffices to describe diffusion data in this region. In the following data analysis, we fix the "hydration number" to $n=6$, keeping $D_1/D_0$ as the independent variable.

Figure 6 shows contours of constant $D_{iso}/D_0$ in the $D_1/D_0$-$n$ plane for fixed $\rho$ and $\phi$. The dashed curves correspond to $\phi=0.25$ and $\rho=4$. Variation of $\phi$ and/or $\rho$ within the experimentally relevant range does not significantly alter the shape of the contours, although they then correspond to different $D_{iso}/D_0$ values. The solid curves in Fig. 6 were calculated at the volume fractions of the four samples studied at $T=T_{NI}-2.5$ K and with the corresponding derived aspect ratios (cf. Sec. IV C). The near coincidence of these curves demonstrates that $D_{iso}/D_0$ can be described with one independent hydration parameter. For example, the two $(n,D_1/D_0)$ pairs (6, 0.40) and (10, 0.63) yield the same $D_{iso}/D_0$ for each sample, although $D_{iso}/D_0$ varies from 0.67 to 0.79 among the four samples.

In the preceding discussion of the obstruction and hydration effects, we have tacitly assumed that the micelles are stationary. While this is not strictly true, we demonstrate in Appendix C that the effect of micelle diffusion on the measured water diffusion coefficients is entirely negligible.

## IV. EXPERIMENTAL RESULTS

### A. General considerations

The relative diffusion coefficients in the crystal frame, $D_{\parallel}^{C}$ and $D_{\perp}^{C}$, were determined at 18 $(T,\phi)$ points in the nematic phase [cf. Fig. 1(b)]. At each $(T,\phi)$ point, there are three independent parameters to be determined: the micellar aspect ratio $\rho$, the orientational order parameter $S$, and the relative local diffusivity of hydration water, $D_1/D_0$. The value of the latter parameter depends on the chosen "hydration number," which we fix at $n=6$ (cf. Sec. III C). These three parameters clearly cannot be determined at any $(T,\phi)$ point from only two observables.

Being a local property, $D_1/D_0$ should not depend on the micelle volume fraction $\phi$. (In the investigated range, $\phi\approx0.2$–$0.3$, the hydration layers of adjacent micelles do not overlap.) Furthermore, although both $D_1$ and $D_0$ increase with temperature, their ratio should not vary significantly over the investigated 27-K range. Indeed, in the defect-free lamellar and hexagonal phases of the potassium palmitate-water system, where the lateral water diffusion coefficient only reflects hydration effects, the activation energy for the observed water self-diffusion coefficient was found to be the same as that for bulk water at all investigated compositions

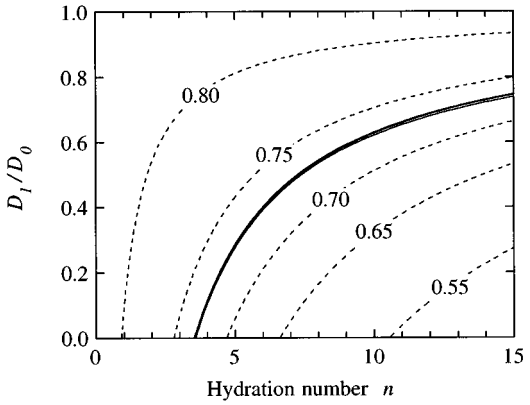


FIG. 6. Contours of constant $D_{iso}/D_0$ (as indicated) for oblate spheroids of aspect ratio $\rho=4$ at volume fraction $\phi=0.25$ (dashed curves). The nearly coincident solid curves refer to four investigated samples ($\phi=0.197$, 0.244, 0.283, and 0.307) $T=T_{NI}-2.5$ K and with aspect ratios as derived from the experimental data ($\rho=3.28$, 3.96, 4.40, and 4.57).

(from 6 to 44 water molecules per amphiphile) [31,32]. Further support for the notion of a temperature-independent $D_1/D_0$ ratio is provided by the present diffusion data (cf. Sec. IV B).

Even with a universal $D_1/D_0$ value, the number of unknowns (37) exceeds the number of observables (36). We therefore proceed as follows. Inserting the experimental $D_{iso}/D_0$ and $\alpha_C$ data in the theoretical relations of Sec. III, we calculate $\rho$ and $S$ as functions of $D_1/D_0$ for each of the 18 $(T,\phi)$ points. The results of such calculations are shown in Fig. 7 for the 2 $(T,\phi)$ points that yield the maximum and minimum $S$ values. Since the order parameter $S$ cannot exceed unity, the data evidently require that $D_1/D_0>0.33$. This condition provides a lower bound on the aspect ratio: $\rho>2.7$ and $\rho>4.0$ for the more dilute and the more concentrated sample, respectively. For the following data analysis, we shall take $D_1/D_0=0.40$. The largest order parameter in our nematic data set then becomes $S=0.79\pm0.06$, corresponding

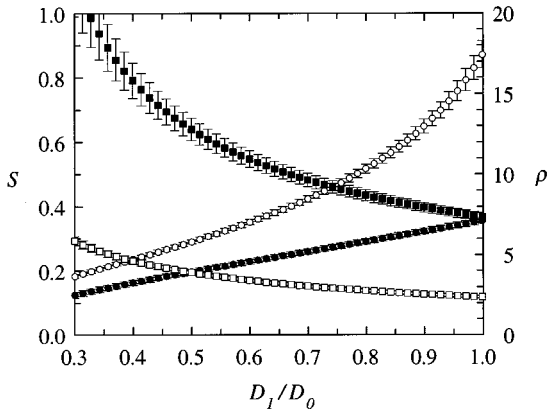


FIG. 7. Order parameter $S$ (squares), and aspect ratio $\rho$ (circles), vs $D_1/D_0$ ($n=6$) for two samples: $\phi=0.197$, $T=T_{NI}-4.5$ K (filled symbols) and $\phi=0.283$, $T=T_{NI}-0.5$ K (open symbols). The bars represent the propagated experimental error.

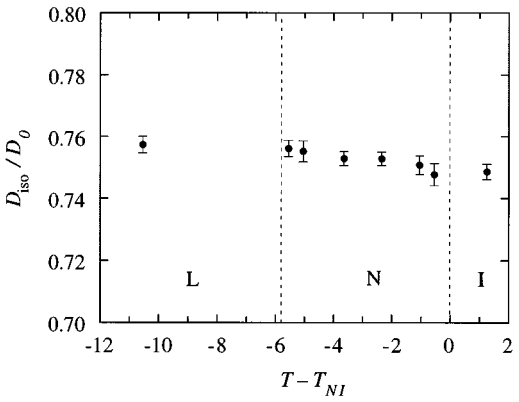


FIG. 8. Temperature variation of the relative, isotropically averaged, water self-diffusion coefficient, $D_{iso}/D_0$, for the $\phi=0.227$ sample in the lamellar ($L$), nematic ($N$), and isotropic ($I$) phases. The bars represent the experimental error.

to the $\phi=0.197$ sample at a temperature ca. 1 K above the $N$-$L$ transition ($T=T_{NI}-4.5$ K). (If also the lamellar phase contains oblate-spheroidal micelles [2,5], the value $D_1/D_0=0.40$ yields $S=0.89\pm0.04$ at 4.75 K below the $N$-$L$ transition.) Order parameters near 0.8 have been reported for nematic phases ca. 5 K below $T_{NI}$ in other systems [33,34]. Furthermore, the value $D_1/D_0=0.40$ is, as expected, not far from the ratio of rotational correlation times, $\tau_1/\tau_0\approx0.3$ (for $n=6$), determined for water in micellar solutions of potassium and cesium alkanoates [35]. Finally, we stress that all trends reported here of $\rho$ and $S$ as functions of $\phi$ and $T$ are unaffected by physically reasonable variations of $D_1/D_0$.

### B. Temperature dependence of micelle size and order parameter

In this subsection, we analyze the diffusion data from the sample at volume fraction $\phi=0.227$, on which the most detailed temperature study was performed. The diffusion data, in the form of $D_{iso}/D_0$ and $\alpha_C$, are shown in Figs. 8 and 9. (As discussed in Sec. III A, this mode of presentation is more informative than that of Fig. 3.)

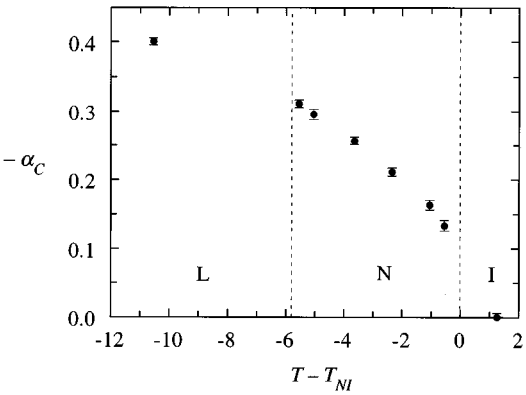


FIG. 9. Temperature variation of the anisotropy $\alpha_C$ of the water self-diffusion tensor for the $\phi=0.227$ sample in the lamellar ($L$), nematic ($N$), and isotropic ($I$) phases. The bars represent the experimental error.

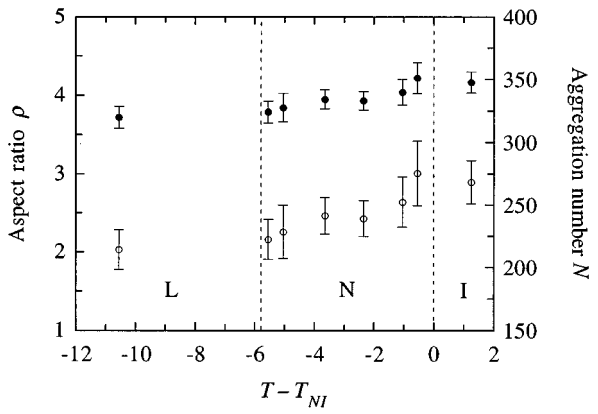


FIG. 10. Temperature variation of the micellar aspect ratio $\rho$ (●) derived from $D_{iso}/D_0$, for the $\phi=0.227$ sample in the lamellar ($L$), nematic ($N$), and isotropic ($I$) phases. The micellar aggregation number $N$ (○) was calculated from $\rho$ assuming a minor semiaxis of 11 Å. The bars represent the propagated experimental error.

The most conspicuous feature of these data is the remarkable invariance of $D_{iso}/D_0$; it decreases by a mere 1.2% on going from a point deep into the lamellar phase, across the nematic phase, and into the isotropic phase. (This highly significant observation is not apparent from Fig. 3.) The only reasonable interpretation of this invariance is that the microstructure varies very little with temperature and that it is virtually the same in all three phases at the same volume fraction. This conclusion should hold whatever the geometry of the microstructure.

With the aid of the oblate-spheroidal micelle model, with $n=6$ and $D_1/D_0=0.40$ (cf. Secs. III and IV A), we can transform the data in Figs. 8 and 9 into the parameters $\rho$ and $S$. The results are shown in Figs. 10 and 11. The observed 1.2% decrease of $D_{iso}/D_0$ translates into a small but significant increase of micelle size, from $\rho=3.7\pm0.1$ in the lamellar phase to $\rho=4.2\pm0.1$ in the isotropic phase, or, in terms of the micellar aggregation number $N$, from $N=210\pm15$ to $270\pm15$. (The minor semiaxis of the oblate-spheroidal micelle is here fixed at the conventional value of 11 Å.) Within the nematic phase, the aggregation number increases by ca. 25%.

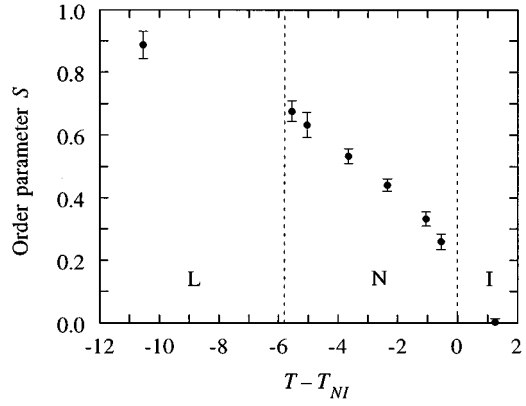


FIG. 11. Temperature variation of the orientational order parameter $S$ derived from $\rho$ and $\alpha_C$, for the $\phi=0.227$ sample in the lamellar ($L$), nematic ($N$), and isotropic ($I$) phases. The bars represent the propagated experimental error.

In contrast to the modest variation in the size of the micelles, their orientational order varies strongly across the 5.8-K range of the nematic phase. The order parameter decreases essentially linearly with temperature up to ca. 1 K below the $N$-$I$ transition, whereafter it seems to drop faster. Although we have not approached $T_{NI}$ closer than 0.5 K, it appears that $S<0.2$ at $T_{NI}$. The strong temperature dependence of $S$ found here, much stronger than in molecular thermotropic nematics [36], is particularly interesting in view of the near-invariant micelle size (cf. Sec. V D).

It is pertinent to ask whether the small increase in micelle shape with temperature found here might be an artifact of the constraint imposed on $D_1/D_0$. Indeed, it is even conceivable that the near invariance of $D_{iso}/D_0$ results from canceling effects of temperature variations in $D_1/D_0$ and $\rho$. In the range of interest, $D_{iso}/D_0$ increases linearly with $D_1/D_0$ and decreases slightly weaker than linearly with $\rho$ (cf. Fig. 4). In terms of $D_{iso}/D_0$, a given relative variation of $\rho$ at fixed $D_1/D_0$ thus corresponds to a slightly smaller relative variation of $D_1/D_0$ at fixed $\rho$. Since $D_0$ varies by 33% [37] over the temperature range of Fig. 8, the variation of $D_1/D_0$ should not exceed a few percent. A significant variation of the microstructure, therefore, cannot be masked by any reasonable variation of $D_1/D_0$. Furthermore, to account for the small decrease of $D_{iso}/D_0$ with temperature in terms of a variation of $D_1/D_0$ at fixed $\rho$, rather than the converse, $D_1/D_0$ must decrease by 15% with increasing temperature. This is not only an order of magnitude larger than expected, but also in the wrong direction. (If anything, $D_1$ should have a higher activation energy than $D_0$.)

### C. Concentration dependence of micelle size and order parameter

Four samples, with the volume fraction ranging from 0.197 to 0.307, were each studied at three temperatures, 0.5, 2.5, and 4.5 K below $T_{NI}$. The results for $D_{iso}/D_0$ and $\alpha_C$ are shown in Figs. 12 and 13. The $D_{iso}/D_0$ data display the expected decrease with $\phi$, due to increasing obstruction and hydration volumes, but do not show the systematic temperature dependence that would be expected if $D_1/D_0$ varied significantly with (absolute) temperature. The observed temperature variation is barely significant and can be accounted for by minute variations of the micelle shape, as for the $\phi=0.227$ sample.

Translating the $D_{iso}/D_0$ and $\alpha_C$ data to $\rho$ and $S$ as before, we obtain the intriguing results shown in Figs. 14 and 15. Whereas the temperature dependence of $\rho$ was barely significant, Fig. 14 reveals a substantial variation with volume fraction: the micelle volume is doubled as $\phi$ goes from 0.2 to 0.3. For a fixed number density of micelles that grow in two dimensions, the micelle volume should increase by only 50% over this $\phi$ range. While the trend is clearly significant, the absolute value of the aggregation numbers in Fig. 14 is somewhat model dependent. An analogous data analysis for hemitoroidal disks, using simulation results for $D_{iso}/D_0$ and $\alpha_M$ [20], yields aggregation numbers that are 20–30% larger than for oblate spheroids if $S$ is taken to be the same for the two geometries.

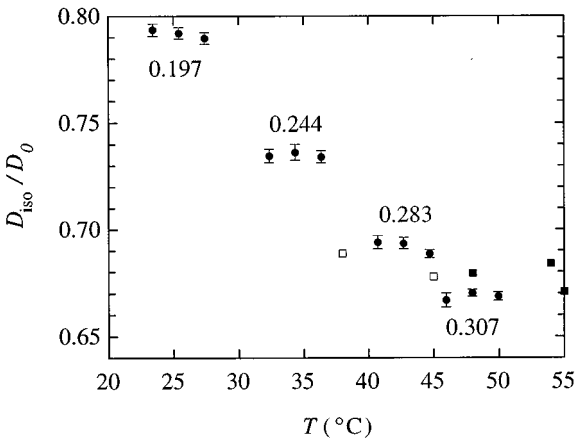


FIG. 12. Variation of the relative, isotropically averaged, water self-diffusion coefficient, $D_{iso}/D_0$, with absolute temperature for four nematic samples at the indicated micelle volume fractions. The bars represent the experimental error. The squares refer to data reported by Chung and Prestegard [17] for a sample at $\phi=0.305$ in the nematic (■) and lamellar (□) phases.

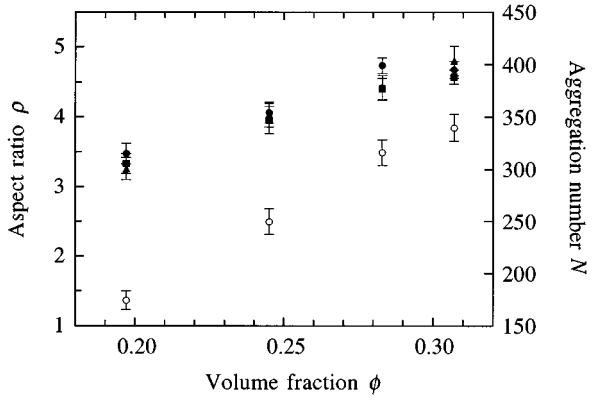


FIG. 14. Variation of the micellar aspect ratio $\rho$ derived from $D_{iso}/D_0$, with the micelle volume fraction $\phi$ for four nematic samples at relative temperatures, $T-T_{NI}=-0.5$ K (●), $-2.5$ K (■), and $-4.5$ K (▲). The micellar aggregation number $N$ (○) was calculated from the average $\rho$ assuming a minor semiaxis of 11 Å. The bars represent the propagated experimental error.

Micellar growth and increased crowding are both expected to enhance the orientational order of the nematic phase at higher volume fractions. Figure 15, however, reveals a clearly significant trend in the opposite direction. While the decrease of $S$ with $\phi$ is modest near $T_{NI}$, it is quite strong near $T_{NL}$. We emphasize again that the uncertainty about the precise value of $D_1/D_0$ cannot reverse this trend. Moreover, since $D_1/D_0$ is a local property, it should not depend on $\phi$. A rationalization of the unexpected order reduction at high $\phi$ in terms of intermicellar interactions is proposed in Sec. V D.

### D. Quadrupole splitting

The water $^2$H quadrupole splitting was determined, simultaneously with the diffusion measurements, from the Fourier transform of the free induction decay following the spin echo. The $^2$H doublet spectrum and its frequency splitting not only serve as a convenient phase indicator and intrinsic temperature reference (cf. Sec. II B), but also contain information about micelle shape and orientational order. The $^2$H quadrupole splitting $\nu_Q$ from a magnetically aligned, uniaxial phase with positive diamagnetic susceptibility is given by [38]

$$\nu_Q=\tfrac{3}{2}f\overline{\chi S}A=\frac{n_Q\overline{\chi S}A}{8(1/\phi-1)}, \tag{4.1}$$

where $f$ is the fraction of orientationally ordered water molecules ($n_Q$ water molecules per CsPFO molecule), with a residual quadrupole coupling constant $\overline{\chi}$ partially averaged by local reorientation at the micelle surface [39]. (Being operationally defined, the hydration numbers $n_Q$ and $n$ are not necessarily equal.)

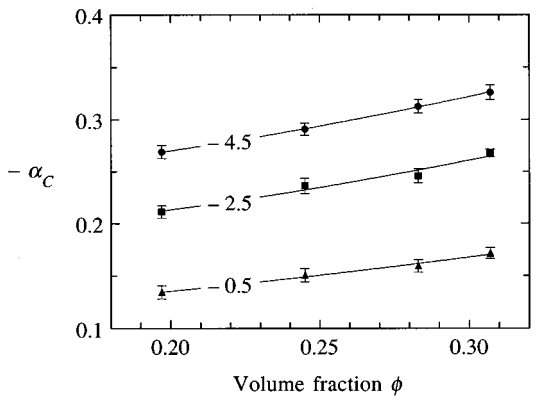


FIG. 13. Variation of the anisotropy $\alpha_C$ of the water self-diffusion tensor with the micelle volume fraction $\phi$ for four nematic samples at the indicated relative temperatures, $T-T_{NI}$. The curves merely serve to guide the eye. The bars represent the experimental error.

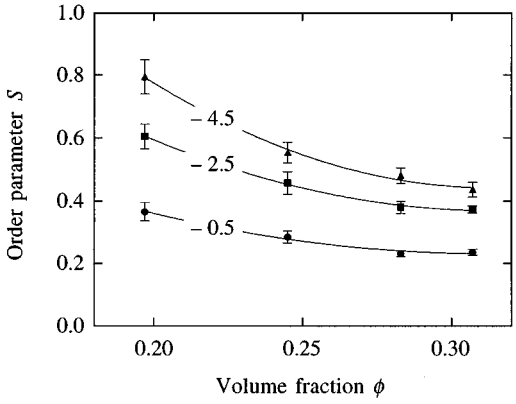


FIG. 15. Variation of the orientational order parameter $S$ derived from $\rho$ and $\alpha_C$, with the micelle volume fraction $\phi$ for four nematic samples at the indicated relative temperatures, $T-T_{NI}$. The curves merely serve to guide the eye. The bars represent the propagated experimental error.

Unlike the ratio $D_1/D_0$, the residual quadrupole coupling constant $\overline{\chi}$ is expected to vary significantly with temperature. For a sample with $\phi=0.30$, the water $^2$H and $^{17}$O and the counterion $^{133}$Cs quadrupole splittings were all measured over a 16-K interval spanning the lamellar and nematic phases (data not shown). The ratio of the water splittings was nearly constant, $\nu_Q(^{17}\mathrm{O})/\nu_Q(^2\mathrm{H})=5.8\pm0.1$, as found in most systems and explained by the near degeneracy of the electric field gradient tensors at the $^2$H and $^{17}$O nuclei [39]. In contrast, the ratio $\nu_Q(^{133}\mathrm{Cs})/\nu_Q(^2\mathrm{H})$ decreases linearly by 9% over a 5-K interval in the nematic phase. Since the counterion $\overline{\chi}$ should vary little with temperature [40], we expect $\overline{\chi}(^2\mathrm{H})$ to increase by ca. 50% over the 27-K temperature range investigated here.

The shape function $A$ in Eq. (4.1) is the second-rank orientational order parameter $\langle P_2(\cos v)\rangle$ associated with the angle $v$ between the local surface normal and the symmetry axis of the (assumed uniaxial) micelle, and the average is taken over the surface of the micelle. If the orientational perturbation in the hydration region is uniform over the micelle surface, then $A$ is a purely geometrical quantity, readily calculated for any uniaxial microstructure. In contrast to the obstruction factors, $D_{\parallel}^{M}/D_0$ and $D_{\perp}^{M}/D_0$, which are not sensitive to the detailed shape of the micelle [20], the shape factor $A$ reflects the curvature of the micelle surface and, hence, differs substantially between, e.g., oblate spheroids [3,41,42] and hemitoroidal disks [34].

It may be thought that the quadrupole splitting could be combined with diffusion data to yield unique values of $\rho$ and $S$ (without having to assign a value for $D_1/D_0$). This is not a viable approach, however, since each measured $\nu_Q$ value adds another unknown: $n_Q\overline{\chi}(T)$. The $^{133}$Cs splitting is not likely to be a better candidate, because, although $\overline{\chi}(^{133}\mathrm{Cs})$ should vary less with temperature, the nonuniform surface distribution of counterions effectively introduces another parameter [43].

Despite these complications, the water $^2$H quadrupole splitting can, to some extent, serve as a check on the interpretation of the diffusion data. Inserting the $\rho$ and $S$ values derived from the diffusion data (cf. Figs. 14 and 15) into Eq. (4.1), with the shape factor $A(\rho)$ for oblate spheroids [3,41,42], we can thus calculate the quantity $n_Q\overline{\chi}$ for each $(T,\phi)$ point. The result, shown in Fig. 16, is indeed consistent with the available information about the quadrupole coupling constant. First, the magnitude of $n_Q\overline{\chi}$ is in the range expected on the basis of the value, $n_Q\overline{\chi}=27$ kHz, reported for the lamellar phases in the potassium and rubidium octanoate-water systems [44]. (If the analogous analysis is performed for hemitoroidal disks, the $n_Q\overline{\chi}$ values in Fig. 16 become 20–25% larger.) Second, data from samples at different volume fractions fall on the same line, as expected since $\overline{\chi}(^2\mathrm{H})$ is a local property and, hence, should not depend on $\phi$. Third, $\overline{\chi}(^2\mathrm{H})$ increases linearly with temperature as predicted from the $\nu_Q(^{133}\mathrm{Cs})/\nu_Q(^2\mathrm{H})$ ratio. In fact, the total increase of $\overline{\chi}(^2\mathrm{H})$ is just about the predicted 50% (cf. above). These observations clearly support our interpretation of the diffusion data.

The notion of an essentially temperature-independent microstructure emerging from the diffusion data (cf. Fig. 8) is also supported by the temperature variation of $\nu_Q$ for the $\phi=0.227$ sample. According to the analysis in Sec. IV B,

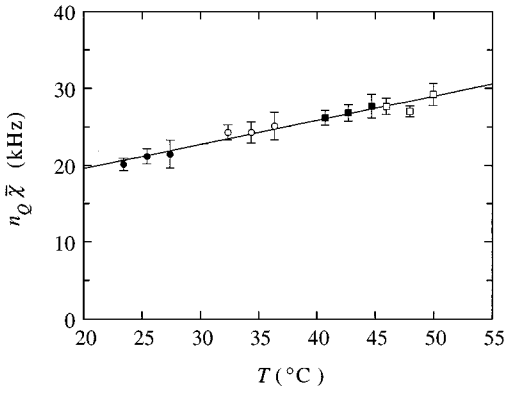


FIG. 16. Temperature variation of the quantity $n_Q\overline{\chi}$ derived from the water $^2$H quadrupole splitting and the $\rho$ and $S$ values obtained from the diffusion data. The symbols refer to samples of different volume fraction, $\phi=0.197$ (●), 0.244 (○), 0.283 (■), and 0.307 (□). The bars represent the propagated experimental error.

about 90% of the temperature variation in the diffusion anisotropy, $\alpha_C$, across the nematic phase is due to the strong temperature dependence of $S$. Since $\nu_Q$ is also proportional to $S$, we expect, for a temperature-invariant microstructure, that the two observables $\nu_Q$ and $\alpha_C$ should exhibit the same relative variation with temperature. As seen from Fig. 17, this is very nearly the case. (The quantities $-\alpha_M$, $A$, and $n_Q\overline{\chi}$ all increase by ca. 10% in this range.) Since the flow-related obstruction anisotropy $\alpha_M$ and the curvature-related shape factor $A$ reflect quite different aspects of the micelle geometry (cf. inset in Fig. 17), a substantial variation of the microstructure across the nematic phase would surely have been detected as a qualitative difference in the variations of $\alpha_C$ and $\nu_Q$ with temperature.

While the ratio $-\alpha_C/\nu_Q$ is nearly constant for the data shown in Fig. 17, we have consistently found that it drops abruptly as $T_{NI}$ is approached within 0.5 K (data not shown). We ascribe this effect, not to a variation of the microstruc-

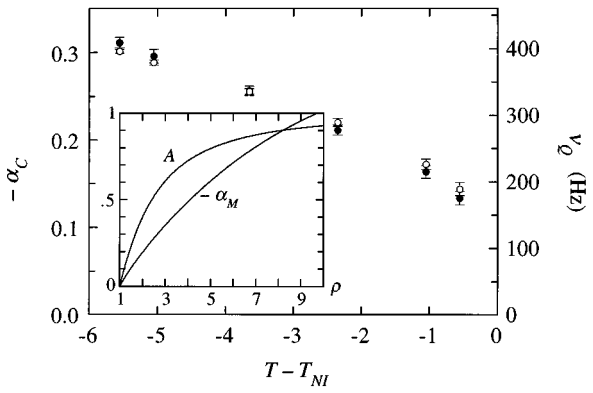


FIG. 17. Temperature variation of the water diffusion anisotropy $\alpha_C$ (●) and the water $^2$H quadrupole splitting $\nu_Q$ (○) in the nematic phase of the $\phi=0.227$ sample. The bars represent the experimental error. The inset shows the variation of the shape factor $A$ and the micelle-frame diffusion anisotropy $\alpha_M$ with the aspect ratio $\rho$ of an oblate spheroid ($\phi=0.227$, $n=6$, $D_1/D_0=0.4$).

ture, but to slow director fluctuations. Near $T_{NI}$, a substantial fraction of the orientational disorder in the nematic phase is due to collective director fluctuations [45]. If some of the director fluctuation modes are slow on the timescale of the quadrupole coupling, motional averaging of the quadrupole frequency will be incomplete. The splitting, $\nu_Q$, then yields an apparent order parameter that is larger than the completely averaged $S$ probed on the longer timescale of the diffusion experiment.

## V. DISCUSSION

Information about the microstructure of the nematic and lamellar phases in the CsPFO-water system has come mainly from measurements of x-ray and neutron scattering [5–9], electrical conductivity [5,10–15], and water diffusion [16–18]. In all cases, the interpretation of experimental data is model dependent to some extent. While the accumulated body of data is impressive, their interpretation thus remains somewhat controversial. In the following, we examine whether our results are consistent with previously reported data and interpretations. We then briefly discuss the implications of our results for the theoretical understanding of the nematic phase in the CsPFO-water system.

### A. Water self-diffusion

The first indication of an unusual microstructure in the lamellar phase of the $Cs^+$, $NH_4^+$, and $Li^+$ PFO-water systems was provided by $^1$H PGSE NMR measurements of the water diffusion anisotropy [16,46]. Similar data were later reported for the lamellar phase in the $NH_4^+$ perfluorononanoate-water [47] and CsPFO-water [18] systems. The water diffusion anisotropy in the nematic phase, however, has only recently been measured [17].

Chung and Prestegard (CP) [17] studied the water diffusion in the nematic and lamellar phases of the CsPFO-$D_2O$ system at $\phi=0.305$, corresponding to our most concentrated sample. However, the transition temperature, $T_{NI}=328$ K, as reported for their sample is 6 K higher than the accepted value [3,4]. Furthermore, the sample studied by CP had a significantly larger nematic range (8 K) than expected (5–6 K) at this composition [3,4]. Their results for $D_{\rm iso}/D_0$, included in Fig. 12, are not markedly different from ours. (Since the experimental accuracy was not specified by CP, it is not possible to say whether the small difference is significant.) However, the diffusion anisotropy reported by CP is of significantly larger magnitude than ours, e.g., $\alpha_C=-0.315$ at $T\approx T_{NI}$ as compared to our value $\alpha_C=-0.171\pm0.005$ at 0.5 K below $T_{NI}$ (cf. Fig. 13). We believe that this discrepancy is connected with the unexpected phase behavior of the sample studied by CP. (No details of CsPFO purification were given.)

The interpretational framework used by Chung and Prestegard is rather different from ours. For an order parameter $S=0.8$ near $T_{NL}$, taken from the literature [5], the micellar aspect ratio was derived from $\alpha_C$, with the obstruction effect calculated from a lattice walk simulation. For reasons discussed elsewhere [20], however, the simulation procedure used by CP produces incorrect results. Indeed, CP state that their simulated obstruction anisotropy $\alpha_M$ reaches an asymptotic (large $\rho$) value of $-0.44$ at $\phi=0.37$, while it is intuitively clear, and follows from the relations given in Sec. III, that $\alpha_M$ must tend to the lamellar limiting value of $-3/2$ at any volume fraction. (CP also use a too large micelle volume fraction for their composition.) Being unable to generate an obstruction anisotropy of sufficient magnitude to account for the measured $\alpha_C$, CP invoked an anisotropic diffusion tensor within the hydration region. With a more accurate description of the obstruction effect, this *ad hoc* modification is unnecessary.

In the recent $^1$H PGSE water diffusion study by Holmes *et al.* (HSHD) [18], $D_{\rm iso}/D_0$ and $\alpha_C$ were determined only in the lamellar and isotropic phases of the CsPFO-$H_2O$ system. At a volume fraction $\phi=0.305$, corresponding to our most concentrated sample, they obtained $D_{\rm iso}/D_0=0.67\pm0.01$ from 15 K below $T_{NL}$ to 20 K above $T_{NI}$. This coincides with our result for the intermediate nematic phase (cf. Fig. 12), although only 5% accuracy was claimed by HSHD. In the presence of 4 wt % CsCl, $D_{\rm iso}/D_0$ was found to decrease to $0.64\pm0.02$ in the same temperature range. Within the oblate-spheroidal model used here, this corresponds to a salt-induced increase of the micellar aspect ratio from $4.5\pm0.5$ to $8\pm2$. The reported anisotropies correspond to order parameters (assuming oblate-spheroidal micelles) in the range 0.5–0.7 in the lamellar phase, although the propagated error is large. HSHD analyzed their $D_{\rm iso}/D_0$ data in a different way, however, calculating obstruction factors for microstructures inferred from scattering data (cf. below), and assuming that $D_1=0$ and that $D_\perp^M/D_0$ is independent of $\phi$. In our view, it is not possible to exclude an oblate-spheroidal microstructure in the lamellar phase on the basis of the diffusion data presented by HSHD.

### B. Electrical conductivity

Electrical conductivity measurements have been extensively reported from all three phases in the CsPFO-water system [2,5,10–15]. From a phenomenological point of view, the macroscopic conductivity tensor is analogous to the macroscopic water self-diffusion tensor. The isotropically averaged conductivity, $\kappa_{\rm iso}$, and the crystal-frame conductivity anisotropy, $\alpha_C(\kappa)$, are thus defined in full analogy with Eqs. (3.2) and (3.4). At the microscopic level, however, there is a fundamental difference: the dynamics of the $Cs^+$ charge carriers is strongly affected by their long-ranged Coulomb interaction with the highly charged micelles [48], whereas the local dynamics of water molecules are only marginally perturbed by short-ranged interactions at the micelle surface. The effect of local electric fields on the interpretation of conductivity data has not yet been examined in detail.

In several studies [5,10,11,49] the conductivity anisotropy $\alpha_C(\kappa)$ has been used to determine the order parameter $S$, with the obstruction factors calculated from the micellar aspect ratio $\rho$ derived from x-ray data (cf. below). In this approach one assumes that the local-field effect on the conductivity cancels out in $\alpha_C(\kappa)$, whereby

$$\alpha_C(\kappa)=S\alpha_M, \tag{5.1}$$

with $\alpha_M$ the same obstruction anisotropy as in Eq. (3.5). Since the diffusion anisotropy $\alpha_C(D)$ is virtually unaffected by hydration effects (cf. Figs. 5 and 21), it follows that the two methods should yield the same anisotropy, i.e.,

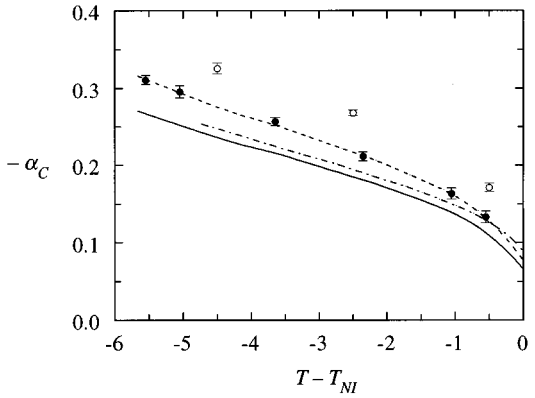


FIG. 18. Water diffusion anisotropy for samples with $\phi=0.227$ (●) and $\phi=0.307$ (○) compared with electrical conductivity anisotropy for samples with $\phi=0.235$ (solid curve, taken from Ref. [2]) and $\phi=0.349$ (dash-dotted curve, taken from Ref. [5]). The dashed curve was obtained by multiplying the solid curve by a factor 1.17.

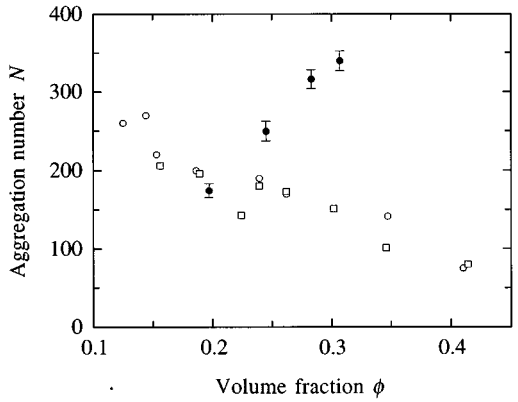


FIG. 19. Variation of the micellar aggregation number $N$ with the micelle volume fraction $\phi$ at fixed relative temperature, $T-T_{NI}$. The results of this study (●) are compared with results at $T=T_{NI}$ derived from x-ray scattering data by Boden *et al.* (○) [2] and by Holmes *et al.* (□) [9].

$\alpha_C(\kappa)=\alpha_C(D)$, provided that the local-field effect on $\alpha_C(\kappa)$ is negligible. To test this assumption, we compare in Fig. 18 the conductivity anisotropy (at $\phi=0.235$ and 0.349) reported by Boden *et al.* [2,5] with the diffusion anisotropy (at $\phi=0.227$ and 0.307) obtained here. Comparing the two data sets at the lower volume fractions, we find a 17% difference over the whole nematic range. (If data from Fig. 13 are used to correct for the small $\phi$ difference between the two samples, the discrepancy becomes 1–2 % larger.) Moreover, whereas the diffusion anisotropy increases markedly with $\phi$, the conductivity anisotropy is almost independent of $\phi$. (The conductivity anisotropy reported by Photinos and Saupe [14] shows even less $\phi$ dependence, but is larger by 30–50% than that reported by Boden *et al.* [2,5] for corresponding samples, suggesting a systematic error in at least one of the studies.) In conclusion, it appears that the local electric fields reduce the conductivity anisotropy substantially, particularly at high volume fractions. By neglecting the local field effect and using Eq. (5.1), one thus obtains a too small order parameter. In previous studies [5,10,11,49], however, the error due to neglect of local fields is partly compensated by the error introduced by calculating the obstruction factor $\alpha_M$ from the effective-medium approximation due to Fricke [28], which substantially underestimates the anisotropy even at $\phi=0.2$ [20].

### C. Small-angle scattering

The size of the discoidal micelles in the nematic phase of the CsPFO-$D_2O$ system have in the past been inferred exclusively from small-angle x-ray and neutron scattering data [2,5–9]. It is of interest to compare these results with those derived here from diffusion data. While we find a barely significant micellar growth with temperature (at $\phi=0.227$), from $N=220\pm15$ to $275\pm25$ (cf. Fig. 10), x-ray scattering data have been interpreted in terms of a modest *decrease* of $N$ with increasing temperature: from 140 to 115 at $\phi=0.351$ [5], and from 200 to 145 at $\phi=0.305$ [9]. A more striking discrepancy is found for the variation of micelle size with volume fraction at fixed relative temperature. As shown in Fig. 19, the micelle size deduced from scattering data *decreases* markedly with $\phi$ at $T_{NI}$, while we find a strong micellar growth with $\phi$ at fixed $T-T_{NI}$.

The aggregation number was derived from scattering data using the relation [5–9]

$$N=\frac{2}{\sqrt{3}}\frac{\phi}{V_{\mathrm{CsPFO}}}d_{\parallel}d_{\perp}^2, \tag{5.2}$$

where $V_{\mathrm{CsPFO}}=360$ Å$^3$ is the amphiphile volume, while $d_{\parallel}$ and $d_{\perp}$ are the characteristic spacings parallel and perpendicular to the director, derived from the meridional and equatorial reflections, respectively. The numerical factor in Eq. (5.2) comes from the assumption that the micelles in the nematic phase are hexagonally arranged on parallel planes, with $d_{\parallel}$ the interplanar spacing and $d_{\perp}$ the in-plane spacing between the 11 lines. While this is a rather crude idealization of the positionally disordered nematic phase, assigning the micelles to any other lattice would merely modify the numerical factor in Eq. (5.2) without affecting the trends of $N$ versus $T$ or $\phi$.

In our opinion, a potentially more serious problem with the interpretation of the scattering data is the effect of orientational order. The diffraction pattern obtained from a small-angle scattering experiment on an aligned nematic micellar phase is due to positional correlations between pairs of scattering centers in the micelles. These correlations depend, in an inseparable way, on positional and orientational micelle pair correlations [50]. Given the strong variation of $S$ with temperature across the nematic phase and the insignificant variation of the microstructure, it appears likely that the observed evolution of the diffraction pattern is largely due to variations in orientational order. The interpretation of the apparent spacings $d_{\parallel}$ and $d_{\perp}$ may then not be so straightforward as generally assumed.

### D. Experiment versus theory

The theoretical understanding of the microstructure in nematic micellar phases is, at best, incomplete. Statistical-

mechanical treatments have so far been limited to rather crude hard-particle models [51–56]. On the basis of scattering and conductivity data from the nematic phase in the CsPFO/$D_2O$ system, it has previously been concluded [2,5,6,9] that (i) the aggregation number $N$ decreases with $T$ at fixed $\phi$, (ii) $N$ decreases with $\phi$ at fixed $T-T_{NI}$, and (iii) the orientational order parameter $S$ increases with $\phi$ at fixed $T-T_{NI}$. In the only theoretical study directly addressing a discotic nematic phase, Taylor and Herzfeld reproduced all these trends [53,54]. It is thus somewhat disconcerting that the present diffusion data reverse all these trends. The only one of our trends that was reproduced by the model calculations is the strong increase of $S$ with decreasing $T$ at fixed $\phi$. In the theoretical study, however, this increase of $S$ was due entirely to a growth-alignment coupling. Since the hard-disk model is an athermal system, the order parameter can increase only if the micelles grow. This mechanism is not consistent with our results, which indicate that the strong increase of $S$ is accompanied by a (small) *reduction* of the micelle size.

We believe that the qualitative discrepancies between the present experimental results and the theoretical predictions based on hard-particle models are due to the omission in these models of the anisotropic electrical double-layer repulsion [57,58], which surely must play a decisive role in these dense and highly charged systems. The importance of electrostatic interactions is clearly indicated by the large observed salt effect on the stability and microstructure of the nematic phase [7,59]. Three aspects of the orientation-dependent electrostatic micelle-micelle interaction are particularly germane to the present discussion. First, since the potential is soft it can account for a temperature variation of $S$ even at fixed micelle size, as seems to be very nearly the case. Second, the dominant contributions to the electrostatic interaction depend on the orientation of the intermicellar vector with respect to the director (for fixed micelle orientations). These contributions are therefore not accounted for in the classical Maier-Saupe theory [60], which implicitly assumes that the micellar pair correlation is spherically symmetric [36]. This may explain why the observed temperature dependence of $S$ is much stronger than the universal $S(T)$ profile predicted by this mean-field theory and obeyed reasonably well by most molecular nematic phases (without dominant electrostatic interactions). Third, the leading anisotropic terms in a multipole expansion of the double-layer interaction between centrosymmetric micelles is the charge-quadrupole and quadrupole-quadrupole interactions [58]. The latter interaction, which becomes relatively more important at short separations, opposes the alignment of adjacent micelles. This observation may explain why $S$ decreases with increasing volume fraction (cf Fig. 15). Since the micellar quadrupole moment increases quadratically with $N$ but the charge only linearly, the observed micellar growth (cf. Fig. 14) would make this mechanism even more effective. In the Maier-Saupe theory, the order parameter at $T_{NI}$ is independent of volume fraction. The results in Fig. 15 suggest that this may actually be the case in the present system, but they also indicate that $S(T_{NI})$ is far below the mean-field value of 0.429.


## ACKNOWLEDGMENTS

We are grateful to Lennart Nilsson and Per-Ola Quist for valuable assistance with gradient coil construction and CsPFO preparation, respectively. This work was supported by the Swedish Natural Science Research Council.


## APPENDIX A: EFFECT OF HYDRATION ON WATER DIFFUSION IN A DISCOTIC NEMATIC MICELLAR PHASE

According to the effective cell approximation [29], we represent the nematic phase by an oblate-spheroidal micelle, centered in a confocal cell of the same geometry and with a volume that matches the macroscopic volume fraction $\phi$. Hydration is introduced by ascribing to the region between the micelle surface and another confocal surface a uniform water density $c_1$ and local diffusion coefficient $D_1$, which may differ from the values $c_0$ and $D_0$ assigned to the bulk-like region outside the latter surface. Proceeding as in the case of spherical geometry [29], we obtain

$$D_{\parallel}^{M}/D_0=\frac{1}{1-\Gamma\phi}\left(1-\frac{\phi}{A_{\parallel}+\phi h_c}\right), \tag{A1a}$$

$$D_{\perp}^{M}/D_0=\frac{1}{1-\Gamma\phi}\left(1-\frac{2\phi}{A_{\perp}+\phi(1-h_c)}\right), \tag{A1b}$$

with

$$A_{\parallel}=\frac{(1-h_m)-h_s\Lambda B_{\parallel}}{1+\varphi\Lambda B_{\parallel}}, \tag{A2a}$$

$$A_{\perp}=\frac{(1+h_m)-(1-h_s)\Lambda B_{\perp}/2}{1+\varphi\Lambda B_{\perp}/2}, \tag{A2b}$$

$$B_{\parallel}=(1-h_m)-(1-h_s)/\varphi, \tag{A3a}$$

$$B_{\perp}=(1+h_m)-(1+h_s)/\varphi, \tag{A3b}$$

$$\Lambda=1-\frac{c_1D_1}{c_0D_0}, \tag{A4}$$

$$\Gamma=\varphi+(1-\varphi)c_1/c_0, \tag{A5}$$

$$\varphi=1+V_{\mathrm{hyd}}/V_{\mathrm{mic}}, \tag{A6}$$

with $V_{\mathrm{mic}}$ the micelle volume and $V_{\mathrm{hyd}}$ the volume of the hydration region. Further, $h_m$, $h_c$, and $h_s$ are defined by Eq. (3.10), with $\xi_m$ and $\xi_c$ obtained from Eqs. (3.11) and (3.12), and $\xi_s$ from the analogous relation

$$\xi_s(\xi_s^2+1)=\frac{\varphi\rho^2}{(\rho^2-1)^{3/2}}. \tag{A7}$$

In the data evaluation, we regard the hydration region as composed of pure water at bulk density, i.e., we set $c_1=c_0$, whereby $\Gamma=1$. It is then natural to specify the extent of the hydration region in terms of the ''hydration number,'' $n$, giving the number of dynamically perturbed water molecules

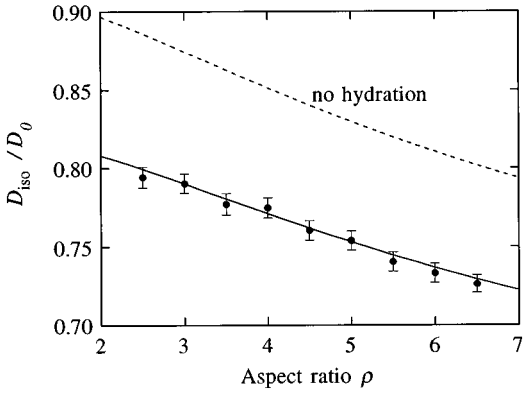


FIG. 20. Shape dependence of the isotropic diffusion coefficient, $D_{iso}/D_0$, for oblate spheroids at volume fraction $\phi=0.2$ with hydration parameters $n=10$ and $D_1/D_0=0.6$. The mean-field approximation (solid curve) is compared with simulation results (●) for an expanded face-centered cubic lattice. The dashed curve represents the mean-field result in the absence of hydration.

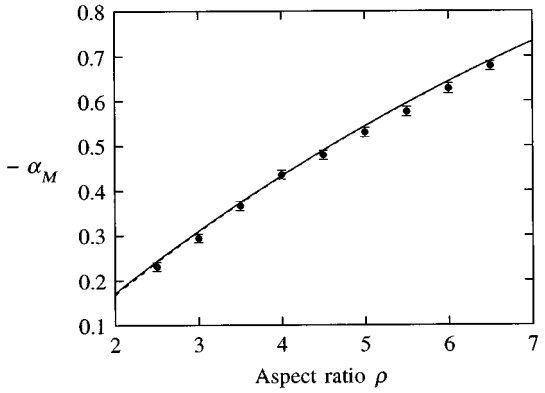


FIG. 21. Shape dependence of the micelle-frame diffusion anisotropy $\alpha_M$ for oblate spheroids at volume fraction $\phi=0.2$ with hydration parameters $n=10$ and $D_1/D_0=0.6$. The mean-field approximation (solid curve) is compared with simulation results (●) for an expanded face-centered cubic lattice. The barely visible dashed curve represents the mean-field result in the absence of hydration.

per CsPFO molecule. With molecular volumes of 30 Å$^3$ for $D_2O$ and 360 Å$^3$ for CsPFO, Eq. (A6) then takes the simple form

$$\varphi=1+n/12. \tag{A8}$$

The pure obstruction factors in Eq. (3.9) are recovered from the preceding results in the absence of hydration ($n=0$, yielding $B_\parallel=B_\perp=0$) as well as in the absence of diffusional retardation ($D_1=D_0$, yielding $\Lambda=0$). Furthermore, in the limit $\rho\to1$, we recover the previously derived result for spherical obstructions with hydration [29].

## APPENDIX B: STOCHASTIC SIMULATION OF WATER DIFFUSION IN A DISCOTIC NEMATIC MICELLAR PHASE

To assess the accuracy of the mean-field approximation, Eqs. (A1)–(A7), for the micelle-frame diffusion coefficients in the presence of hydration, we performed stochastic simulations using an extension of a random-flight procedure described elsewhere [20]. In the simulation, the diffusive motion of a water molecule is modeled as a random flight, where each step vector $\boldsymbol{\delta}$ is chosen from a continuous step vector distribution $f(\boldsymbol{\delta})$. As before [20], we used a truncated spherical distribution with $\boldsymbol{\delta}$ uniformly distributed within a sphere of radius $\Delta$, whereby $\langle\delta^2\rangle=(3/5)\Delta^2$. Since the local diffusion coefficient is proportional to $\langle\delta^2\rangle$, the step length cutoffs for the bulk ($\Delta_0$) and hydration ($\Delta_1$) regions are related by $\Delta_1/\Delta_0=(D_1/D_0)^{1/2}$.

In the simulations reported here, the oblate-spheroidal obstructions were arranged on a lattice constructed by uniformly dilating a face-centered cubic lattice by a factor $\rho$ (the aspect ratio of the obstruction) in two dimensions. The volume fraction was $\phi=0.2$ and the hydration parameters were $n=10$ and $D_1/D_0=0.6$, corresponding closely to the experimental conditions (cf. Fig. 6). As seen from Fig. 20, the mean-field approximation accurately describes the combined obstruction and hydration effects on the isotropically averaged diffusion coefficient, $D_{iso}/D_0$. As in the absence of hydration, this is partly due to a cancellation of errors in $D_\parallel^M$ and $D_\perp^M$. The micelle-frame diffusion anisotropy $\alpha_M$, shown in Fig. 21, is slightly exaggerated in the mean-field approximation. The consequences of this slight difference are, however, negligible compared to the propagated experimental errors in this study. As noted in Sec. II C, the hydration effect on $\alpha_M$ is negligible.

## APPENDIX C: EFFECT OF MICELLE DIFFUSION ON THE MACROSCOPIC WATER DIFFUSION COEFFICIENTS

In the discussion of the obstruction and hydration effects in Sec. III, the micelles were implicitly regarded as stationary. To analyze the effect of micelle diffusion, it is conceptually convenient to consider a reference system of immobile micelles positioned on a lattice. By allowing the micelles to diffuse off the lattice, two distinct effects are introduced. First, the system becomes positionally disordered. The effect of positional disorder on the water diffusion was shown in a recent simulation study [20] to be very small in two dimensions and completely negligible in three dimensions. Second, there is a purely dynamical effect due to water-micelle correlations. This effect can be isolated by considering a system where the micelles undergo instantaneous jumps between neighboring lattice positions. As long as the dynamics are described at a Markovian level (diffusion or jumps), with no reference to particle velocities, the dynamic effect vanishes if the local water diffusion coefficient is uniform (no hydration effect). In another extreme, with $D_1\ll D_{iso}^{mic}$ and $f\ll1$, the hydration water simply moves with the micelle, and

$$D_{iso}=D_{iso}^{stat}+fD_{iso}^{mic}, \tag{C1}$$

with $f$ the fraction hydration water, $D_{iso}^{mic}$ the isotropically averaged micelle diffusion coefficient, and $D_{iso}^{stat}$ that of water

in the case of stationary micelles. For an oblate-spheroidal micelle of aspect ratio $\rho=3.5$ and a minor semiaxis of 11 Å (as for CsPFO), we estimate that $D_{\rm iso}^{\rm mic}/D_{\rm iso}^{\rm stat}\approx 0.03$ at infinite dilution. For the strongly interacting micelles in the nematic phase, we expect this ratio to be an order of magnitude smaller. Moreover, since $D_1$ is really of the same order of magnitude as $D_0$, so that $D_1 \gg D_{\rm iso}^{\rm mic}$, we are very far from the limit where Eq. (C1) applies. In conclusion, the effect of micelle diffusion on the macroscopic water diffusion coefficients in a nematic phase is negligible.


[1] K. D. Lawson and T. J. Flautt, J. Am. Chem. Soc. **89**, 5489 (1967).
[2] N. Boden, in *Micelles, Membranes, Microemulsions, and Monolayers*, edited by W. M. Gelbart, A. Ben-Shaul, and D. Roux (Springer-Verlag, New York, 1994), p. 153.
[3] N. Boden, S. A. Corne, and K. W. Jolley, J. Phys. Chem. **91**, 4092 (1987).
[4] N. Boden, K. W. Jolley, and M. H. Smith, Liq. Cryst. **6**, 481 (1989).
[5] N. Boden, S. A. Corne, M. C. Holmes, P. H. Jackson, D. Parker, and K. W. Jolley, J. Phys. (Paris) **47**, 2135 (1986).
[6] M. C. Holmes, D. J. Reynolds, and N. Boden, J. Phys. Chem. **91**, 5257 (1987).
[7] M. S. Leaver and M. C. Holmes, J. Phys. (France) II **3**, 105 (1993).
[8] M. C. Holmes, A. M. Smith, and M. S. Leaver, J. Phys. (France) II **3**, 1357 (1993).
[9] M. C. Holmes, M. S. Leaver, and A. M. Smith, Langmuir **11**, 356 (1995).
[10] N. Boden, D. Parker, and K. W. Jolley, Mol. Cryst. Liq. Cryst. **152**, 121 (1987).
[11] N. Boden, J. Clements, K. A. Dawson, K. W. Jolley, and D. Parker, Phys. Rev. Lett. **66**, 2883 (1991).
[12] N. Boden and K. W. Jolley, Phys. Rev. A **45**, 8751 (1992).
[13] P. Photinos and A. Saupe, Phys. Rev. A **41**, 954 (1990).
[14] P. Photinos and A. Saupe, Phys. Rev. A **43**, 2890 (1991).
[15] C. Barnes, C. Frank, B. Leybold, and P. Photinos, Phys. Rev. E **48**, 2792 (1993).
[16] G. J. T. Tiddy, J. B. Hayter, A. M. Hecht, and J. W. White, Ber. Bunsenges. Phys. Chem. **78**, 961 (1974).
[17] J. Chung and J. H. Prestegard, J. Phys. Chem. **97**, 9837 (1993).
[18] M. C. Holmes, P. Sotta, Y. Hendrikx, and B. Deloche, J. Phys. (France) II **3**, 1735 (1993).
[19] I. Furó and H. Jóhannesson, J. Magn. Reson. A (to be published).
[20] H. Jóhannesson and B. Halle, J. Chem. Phys. (to be published).
[21] N. Boden, G. R. Hedwig, M. C. Holmes, K. W. Jolley, and D. Parker, Liq. Cryst. **11**, 311 (1992).
[22] P. T. Callaghan, M. A. Le Gros, and D. N. Pinder, J. Chem. Phys. **79**, 6372 (1983).
[23] J. Kärger, H. Pfeifer, and W. Henk, Adv. Magn. Reson. **12**, 1 (1988).
[24] P. T. Callaghan, *Principles of Nuclear Magnetic Resonance Microscopy* (Oxford Univ. Press, Oxford, 1991).
[25] T. J. Norwood, J. Magn. Reson. A **103**, 258 (1993).
[26] P. G. de Gennes and J. Prost, *The Physics of Liquid Crystals*, 2nd ed. (Clarendon, Oxford, 1993).
[27] Z. Hashin and S. Shtrikman, J. Appl. Phys. **33**, 3125 (1962).
[28] H. Fricke, Phys. Rev. **24**, 575 (1924).
[29] Be. Jönsson, H. Wennerström, P. G. Nilsson, and P. Linse, Colloid Polym. Sci. **264**, 77 (1986).
[30] G. Carlström and B. Halle, J. Chem. Soc., Faraday Trans. 1 **85**, 1049 (1989).
[31] G. Chidichimo, D. De Fazio, G. A. Ranieri, and M. Terenzi, Chem. Phys. Lett. **117**, 514 (1985).
[32] G. Chidichimo, D. De Fazio, G. A. Ranieri, and M. Terenzi, Mol. Cryst. Liq. Cryst. **135**, 223 (1986).
[33] P-O. Quist, B. Halle, and I. Furó, J. Chem. Phys. **96**, 3875 (1992).
[34] I. Furó and B. Halle, Phys. Rev. E **51**, 466 (1995).
[35] B. Halle and G. Carlström, J. Phys. Chem. **85**, 2142 (1981).
[36] G. R. Luckhurst, in *The Molecular Physics of Liquid Crystals*, edited by G. R. Luckhurst and G. W. Gray (Academic, London, 1979), p. 85.
[37] R. Mills, J. Phys. Chem. **77**, 685 (1973).
[38] A. Abragam, *The Principles of Nuclear Magnetism* (Clarendon, Oxford, 1961).
[39] B. Halle and H. Wennerström, J. Chem. Phys. **75**, 1928 (1981).
[40] P-O. Quist, B. Halle, and I. Furó, J. Chem. Phys. **95**, 6945 (1991).
[41] M. R. Kuzma, J. Phys. Chem. **89**, 4124 (1985).
[42] B. Halle, J. Chem. Phys. **94**, 3150 (1991).
[43] N. Boden, K. W. Jolley, and M. H. Smith, J. Phys. Chem. **97**, 7678 (1993).
[44] N-O. Persson and B. Lindman, J. Phys. Chem. **79**, 1410 (1975).
[45] C. Rosenblatt, Phys. Rev. A **32**, 1115 (1985).
[46] G. J. T. Tiddy, J. Chem. Soc., Faraday Trans. 1 **73**, 1731 (1977).
[47] G. Chidichimo, L. Coppola, C. La Mesa, G. A. Ranieri, and A. Saupe, Chem. Phys. Lett. **145**, 85 (1988).
[48] D. Stigter, J. Phys. Chem. **83**, 1663 (1979).
[49] N. Boden, J. Clements, K. W. Jolley, D. Parker, and M. H. Smith, J. Chem. Phys. **93**, 9096 (1990).
[50] G. Fröba and J. Kalus, J. Phys. Chem. **99**, 14 450 (1995).
[51] W. M. Gelbart, W. E. McMullen, and A. Ben-Shaul, J. Phys. (Paris) **46**, 1137 (1985).
[52] R. Hentschke and J. Herzfeld, Phys. Rev. A **44**, 1148 (1991).
[53] M. P. Taylor and J. Herzfeld, Phys. Rev. A **43**, 1892 (1991).
[54] M. P. Taylor and J. Herzfeld, J. Phys. Condens. Matter **5**, 2651 (1993).
[55] P. van der Schoot and M. E. Cates, Langmuir **10**, 670 (1994).
[56] P. van der Schoot and M. E. Cates, Europhys. Lett. **25**, 515 (1994).
[57] H. Löwen, J. Chem. Phys. **100**, 6738 (1994).
[58] B. Halle, J. Chem. Phys. **102**, 7238 (1995).
[59] B. Cull, M. Heino, S. H. Lee, S. Kumar, S. S. Keast, and M. E. Neubert, Liq. Cryst. **17**, 507 (1994).
[60] W. Maier and A. Saupe, Z. Naturforsch. **13a**, 564 (1958); **14a**, 882 (1959); **15a**, 287 (1960).